

Alchemical Transformations for Single-Step Hydration Free Energy Calculations

Emilio Gallicchio¹*egallicchio@brooklyn.cuny.edu**Department of Chemistry, Brooklyn College of the City University of New York, New York,**NY; Ph.D. Program in Chemistry, The Graduate Center of the City University of New York, New York,**NY; Ph.D. Program in Biochemistry, The Graduate Center of the City University of New York, New York,**NY*

(Dated: 12 June 2022)

We present a family of alchemical perturbation potentials that allow the calculation of hydration free energy of small to medium-sized molecules in a single perturbation step. We also present a general framework to optimize the parameters of the alchemical perturbation potentials based on avoiding first order pseudo phase transitions along the alchemical path. We illustrate the method for two compounds of increasing size and complexity: ethanol and 1-naphtol. In each case we show that convergence of the hydration free energy is achieved rapidly when conventional approaches fail.

I. INTRODUCTION

The hydration free energy of a compound is defined as the reversible work for transferring one molecule of the compound from the gas phase to the water phase.¹ The hydration free energy is an important characteristic of a substance. For instance it is one of the determinant factors of the water solubility of drug formulations² and of the binding affinity of an inhibitor towards a protein receptor.³ Hydration free energies are most commonly derived from Henry's constant measurements.⁴

Free energies of hydration can also be estimated computationally.⁵ Most commonly this is accomplished by molecular simulations of alchemical transformations in which solute-solvent interactions are progressively turned on. The nature of the alchemical transformation is critical to obtaining reliable results. For compounds other than the smallest solutes, a single direct alchemical process in which the coupling between the solute and the solvent is increased in a simple linear fashion has been found to be problematic for anything other than the smallest solutes (monoatomic atoms and ions, water, methane, etc.).⁶ Some of the problems are due to the singularity of the derivative of the alchemical potential with respect to the charging parameter λ near the decoupled state.⁷ Simple approaches of this kind can also be found to converge slowly due to bottlenecks along the alchemical path caused by poorly sampled conformational equilibria.⁸

These issues have been the subject of intense studies. This collective effort resulted in a set of recommended best practices for alchemical calculations that are commonly employed by the computational chemistry community and that are nowadays implemented in popular molecular simulation software packages.^{5,9} For example, it is generally recommended to split the coupling of the solute and the solvent in two phases, the first in which the volume-exclusion core repulsion and dispersion interactions are turned on, and a second phase in which electrostatic interactions are turned on. Soft-core interatomic potentials are a useful expedient to avoid end-point singularities, especially when volume-exclusion core repulsion terms are introduced. Moreover for large solutes it is also often necessary to introduce one small group of atoms at a time or to

resort to bond-growing processes in which solute atoms are pushed out from a central point rather than directly created in the solvent.

While successful, these strategies add layers of complexity to hydration free energy calculations.¹⁰ Splitting the coupling process in two phases requires specifying two alchemical schedules which are often very different from each other. In addition, this practice relies on simulating a nonphysical intermediate state consisting of the uncharged solute in water which could have very different conformational propensities than the actual solute. It could, for example, undergo hydrophobic collapse. Soft-core potential function implementations are difficult and cumbersome to maintain. In addition, they require additional parameters that need to be tuned according to the nature of the interaction potential.

It would be therefore beneficial to develop more streamlined alchemical protocols that (i) compute the hydration free energy in one continuous transformation process, (ii) that are based on the standard form of interatomic potentials, and (iii) that can be parameterized using a linear progression of the charging parameter λ , while (iv) preserving or improving the rate of equilibration and convergence of free energy estimates relative to mainstream protocols. We present here a method that has all of these characteristics and that has the potential to be widely applicable. The approach is based on the work we carried out recently to optimize binding free energy calculations with implicit solvation.¹¹ This work resulted into the development of a family of single-step alchemical potential energy functions as well as a general framework to optimize them to accelerate conformational sampling and convergence. In the present work we illustrate how the same approach can be employed to evaluate the hydration free energies of small to medium-sized molecule with explicit solvation. As in our original work, the approach is founded on the realization that slow equilibration and convergence is caused by entropic bottlenecks akin to first-order phase transitions that can be circumvented by an appropriate choice of the alchemical potential energy function.

This work is organized as follows. We first review the theoretical and computational protocol developed earlier and then we apply to a model system of hydration in which two

solutes (ethanol and 1-naphtol) are transferred from the gas phase to a water droplet. We show that the optimized protocols yield results consistent with conventional approaches for the small solute ethanol for which they can reach convergence. For the larger solute 1-naphtol, only the optimized protocol can achieve rapid convergence. These promising outcomes pave the way for a novel generation of more efficient and more streamlined single-step alchemical free energy methodologies.

II. THEORY AND METHODS

A. Alchemical Transformations for the Estimation of Hydration Free Energies

Alchemical transformations are based on an alchemical potential energy function that interpolates between the potential energy function U_0 of the starting state and that of the final state U_1 as the progress parameter λ goes, conventionally, from 0 to 1. The most straightforward approach is a linear interpolating function of the form:

$$U_\lambda(x) = U_0(x) + \lambda[U_1(x) - U_0(x)] = U_0(x) + \lambda u(x) \quad (1)$$

where x represents the degrees of freedom of the system and we have introduced the perturbation function

$$u(x) = U_1(x) - U_0(x) \quad (2)$$

which in the case of hydration corresponds to the solute-solvent interaction energy and, critical to the following developments, does not depend on λ .

While straightforward, this simple alchemical potential energy function leads to instabilities and poor convergence especially when volume-exclusions terms are introduced. To address these issues while maintaining as much as possible the same simple framework, we consider the family of alchemical potential energy functions of the form:

$$U_\lambda(x) = U_0(x) + W_\lambda[u_{sc}(x)] \quad (3)$$

where $u_{sc}(x)$, defined below, is a soft-core $C(2)$ -smooth, and one-to-one map of the solute-solvent interaction energy u , and $W_\lambda(u_{sc})$ is an alchemical perturbation function defined such that $W_0(u_{sc}) = 0$ and $W_1(u_{sc}) = u_{sc}$ at $\lambda = 0$ and $\lambda = 1$, respectively. We will consider in this work the linear function $W_\lambda(u) = \lambda u_{sc}$ and the integrated logistic function

$$W_\lambda(u_{sc}) = \frac{\lambda_2 - \lambda_1}{\alpha} \ln \left[1 + e^{-\alpha(u_{sc} - u_0)} \right] + \lambda_2 u_{sc} + w_0 \quad (4)$$

where the parameters λ_2 , λ_1 , α , u_0 , and w_0 are functions of λ . The name of this function comes from the fact that its derivative is the logistic function (also known as Fermi's function):

$$\frac{\partial W_\lambda(u_{sc})}{\partial u_{sc}} = \frac{\lambda_2 - \lambda_1}{1 + e^{-\alpha(u_{sc} - u_0)}} + \lambda_1. \quad (5)$$

The parameters of the integrated logistic function are optimized using the procedure described in reference 11 and is briefly described below.

In this work, we employ the following definition of the soft-core solute-solvent interaction energy¹¹

$$u_{sc}(u) = \begin{cases} u & u \leq 0 \\ u_{\max} f_{sc}(u/u_{\max}) & u > 0 \end{cases} \quad (6)$$

where

$$f_{sc}(y) = \frac{z^a - 1}{z^a + 1}, \quad (7)$$

where $u_{\max} > 0$ is the maximum allowed value of the soft-core solute-solvent interaction energy, $z = 1 + 2y/a + 2(y/a)^2$ and a is an adjustable dimensionless exponent. Here $u_{\max} = 50$ kcal/mol and $a = 1/16$.

We stress that in this approach there are no soft-core modifications of individual interatomic interactions. The soft-core function is applied to the overall solute-solvent interaction energy u evaluated with the standard form of the Coulomb and Lennard-Jones interatomic potentials without soft-core modifications.

To obtain the hydration free energy, a set of samples of the soft-core solute-solvent interaction energies, $u_{sc}(i)$, are collected during molecular dynamics simulations performed at a sequence of λ values between 0 and 1. The free energy profile as a function of λ , $\Delta G(\lambda)$, is obtained by multi-state reweighting¹² using the UWHAM method.¹³ The hydration free energy in the Ben-Naim standard state¹⁴ is by definition the value of free energy profile at $\lambda = 1$, $\Delta G_h^* = \Delta G(1)$.

B. Analytic Theory of Alchemical Transformations

The hydration process is analyzed and optimized using the theory we recently developed for alchemical potential energy function of the form of Eq. (3).¹⁵ The key quantity of this theory is in this case $p_0(u_{sc})$, the probability density of the soft-core solute-solvent interaction energy u_{sc} in the ensemble in which solute and solvent are uncoupled ($\lambda = 0$ in this context). All other quantities of the alchemical transformation can be obtained from $p_0(u_{sc})$.^{16,17} In particular, given $p_0(u_{sc})$, the probability density for the binding energy u_{sc} for the state with perturbation potential $W_\lambda(u_{sc})$ is

$$p_\lambda(u_{sc}) = \frac{1}{K(\lambda)} p_0(u_{sc}) \exp[-\beta W_\lambda(u_{sc})] \quad (8)$$

where $\beta = 1/k_B T$,

$$K(\lambda) = \int_{-\infty}^{+\infty} p_0(u_{sc}) \exp[-\beta W_\lambda(u_{sc})] du_{sc} = \langle \exp[-\beta W_\lambda(u_{sc})] \rangle_{\lambda=0} \quad (9)$$

is the excess component of the equilibrium constant for binding and

$$\Delta G(\lambda) = -\frac{1}{\beta} \ln K(\lambda) \quad (10)$$

is the corresponding free energy profile. Note that for a linear perturbation potential, $W_\lambda(u_{sc}) = \lambda u_{sc}$, Eqs. (9) and (10)

state that the free energy profile is related to the double-sided Laplace transform of $p_\lambda(u_{sc})$.

An analytical description of $p_0(u_{sc})$, and thus of all the quantities derived from it, is available. Briefly (see reference 15 for the full derivation), the theory is based on the assumption that the statistics of, in this case, the solute-solvent interaction energy u is the superposition of two processes, one that describes the sum of many “soft” background solute-solvent interactions and that follows central limit statistics, and another process that describes “hard” atomic collisions and that follows max statistics. The probability density $p_0(u)$ is expressed as the superposition of probability densities of a small number of modes

$$p_0(u) = \sum_i c_i p_{0i}(u) \quad (11)$$

where c_i are adjustable weights summing to 1 and $p_{0i}(u)$ is the probability density corresponding to mode i described analytically as (see reference 15 and appendix A of reference 11 for the derivation):

$$p_{0i}(u) = p_{bi} g(u; \bar{u}_{bi}, \sigma_{bi}) + (1 - p_{bi}) \int_0^{+\infty} p_{WCA}(u'; n_{li}, \varepsilon_i, \tilde{u}_i) g(u - u'; \bar{u}_{bi}, \sigma_{bi}) du' \quad (12)$$

where $g(u; \bar{u}, \sigma)$ is the normalized Gaussian density function of mean \bar{u} and standard deviation σ and

$$p_{WCA}(u; n_l, \varepsilon, \tilde{u}) = n_l \left[1 - \frac{(1 + x_C)^{1/2}}{(1 + x)^{1/2}} \right]^{n_l - 1} \frac{H(u) (1 + x_C)^{1/2}}{4\varepsilon_{LJ} x(1 + x)^{3/2}}, \quad (13)$$

where $x = \sqrt{u/\varepsilon + \tilde{u}/\varepsilon + 1}$ and $x_C = \sqrt{\tilde{u}/\varepsilon + 1}$. The model for each mode i depends on a number of adjustable parameters corresponding to the following physical quantities¹⁵:

- c_i : relative population of mode i
- p_{bi} : probability that no atomic clashes occur while in mode i
- \bar{u}_{bi} : the average background interaction energy of mode i
- σ_{bi} : the standard deviation of background interaction energy of mode i
- n_{li} : the effective number of statistical uncorrelated atoms of the solute in mode i
- ε_i : the effective ε parameter of an hypothetical Lennard-Jones interaction energy potential describing the solute-solvent interaction energy in mode i
- \tilde{u}_i : the solute-solvent interaction energy value above which the collisional energy is not zero in mode i

The parameters above, together with the weights c_i , are varied to fit, using the maximum likelihood criterion, the distributions of the soft-core solute-solvent interaction energy obtained from numerical simulations.¹⁵ The distribution of the soft-core solute-solvent interaction energy $p_0(u_{sc})$ is obtained

from $p_0(u)$ using the standard formula for the change of random variable.¹¹

In this work we use the analytical theory above and the results of trial alchemical simulations to optimize the parameters of the integrated logistic alchemical perturbation potential in Eq. (4).¹¹ Briefly, the procedure consists of running a trial alchemical calculations using the the linear alchemical potential $W_\lambda(u_{sc}) = \lambda u_{sc}$. The set of samples of the soft-core binding energies as a function of λ obtained from the trial simulation are then used to derive a maximum likelihood parameterization of the analytical model for $p_0(u_{sc})$ [Eqs. (11) to (13)]. We developed an application based on the Tensorflow¹⁸ to conduct the maximum likelihood optimization.¹⁹

The analytical form of $p_0(u_{sc})$ so obtained is then analytically differentiated with respect to u_{sc} to obtain the so-called λ -function:

$$\lambda_0(u_{sc}) \equiv \frac{1}{\beta} \frac{\partial \ln p_0(u_{sc})}{\partial u_{sc}}. \quad (14)$$

Because, minima and maxima of $p_\lambda(u_{sc})$ occur when the λ -function and $\partial W_\lambda(u_{sc})/\partial u_{sc}$ intersect¹¹

$$\lambda_0(u_{sc}) = \frac{\partial W_\lambda(u_{sc})}{\partial u_{sc}}, \quad (15)$$

the λ -function can be used as a guide to design alchemical potentials that avoid the occurrence of bimodal distributions that are difficult to converge. The linear alchemical potential $W_\lambda(u_{sc}) = \lambda u_{sc}$ leads to $\partial W_\lambda(u_{sc})/\partial u_{sc} = \lambda = \text{constant}$, which in many cases intersects the λ -function at multiple points. Here we use the integrated logistic alchemical potential and we vary the parameters λ_2 , λ_1 , α , u_0 , and w_0 as a function of λ such that the derivative of the integrated logistic function in Eq. (5) intersects $\lambda_0(u_{sc})$ at a single point at each λ or, when this is not easily achievable, such that it intersects it at nearby points. As thoroughly discussed in reference 11 this procedure removes or reduces the severity of entropic sampling bottlenecks during the alchemical coupling process and enhances conformational sampling efficiency and convergence of the binding free energy estimates.

C. Computational Details

In this work we employ a model of hydration in which solutes are transferred from vacuum to near the center of mass of a water droplet of about 27 Å in diameter composed of 357 TIP3P water molecules (Figure 1). The droplet is confined in a spherical region defined by a flat-bottom harmonic restraining potential centered at the origin and acting on each TIP3P water oxygen atom. The tolerance of the flat-bottom potential was set to 24 Å (to ensure a confinement region of approximately twice the volume of the droplet) and a force constant of 5 kcal/(mol Å²) beyond this tolerance. This model was chosen to illustrate and validate the novel methodology presented here to avoid potential issues with an implementation of the alchemical transfer with periodic boundary conditions.²⁰

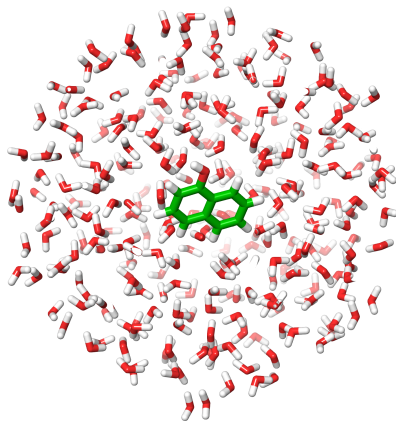


FIG. 1. Illustration of 1-naphthol (green carbon atoms) inserted into the center of the droplet of water employed in this work. Water molecules obscuring the solute are not shown for clarity.

The solutes (ethanol and 1-naphthol) were prepared with Maestro and GAFF/AM1-BCC force field parameters were assigned using the Antechamber program.²¹ Single Decoupling alchemical calculations were prepared using the SDM workflow ([github.com/egallicc/openmm_sdm_workflow.git](https://github.com/egallicc/openmm_sdm_workflow)) using 16 λ steps. The MD calculations employed the OpenMM²² MD engine the SDM integrator plugins ([github.com/rajatkrpal/openmm_sdm_plugin.git](https://github.com/rajatkrpal/openmm_sdm_plugin)) using the OpenCL platform. The ASyncRE software,²³ customized for OpenMM and SDM ([github.com/egallicc/async_re-openmm.git](https://github.com/egallicc/async_re-openmm)), was used for the Hamiltonian Replica Exchange in λ space with an uniform λ schedule between 0 and 1. The λ -dependent parameters used with the integrated logistic potential are listed in Tables III and IV. Molecular dynamics runs were conducted for a minimum of 2 ns per replica with a 1 fs time-step at 300 K, exchanging λ values approximately every 5 ps. A Langevin thermostat at 300 K with a relaxation time constant of 20 ps was used. Binding energy samples and trajectory frames were recorded every 5 ps. Calculations were performed on the XSEDE Comet GPU HPC cluster at the San Diego Supercomputing Center.

In this work, we employ the Hamiltonian Replica Exchange algorithm^{24–27} in alchemical space to accelerate conformational sampling.^{16,28,29} For the calculations reported here, we have employed the asynchronous implementation of Replica Exchange (ASyncRE)²³ with the Gibbs Independence Sampling algorithm for state reassignments.¹¹

III. RESULTS

A. Probability Distributions of the Solute-Solvent Interaction Energy

As discussed in Theory and Methods, the free energy profile is determined by the probability distributions of the perturbation energy (the soft-core solute-solvent interaction energy, u_{sc} , in this case) along the alchemical path. The probability distributions $p_\lambda(u_{sc})$ for some values of λ obtained from the replica exchange simulations of the hydration of ethanol and 1-naphthol with the linear alchemical potential are shown in Figure 2 (dots). At small λ s the distributions are centered around large and unfavorable values of the solute-solvent interaction energy reflecting the fact that atomic clashes are frequent when the solute and solvent are weakly coupled. Conversely, at large λ s solute and solvent are strongly coupled and the solute-solvent interaction energies tend to be favorable. However, the distributions do not uniformly move towards lower values of u_{sc} as λ is progressively increased. Rather, at intermediate values of λ they become bimodal with a trough near $u_{sc} = 0$ separating the weakly decoupled and strongly coupled states. The conversion from weakly coupled to strongly coupled behavior occurs by the transfer of population between the two states rather than by the formation of an homogeneous intermediate state. The transition occurs somewhat gradually in the case of ethanol where the modes corresponding to weakly coupled and strongly coupled states partially overlap when they are in equilibrium near $\lambda = 0.4$ (Figure 2, green curve).

However, the transition occurs much more sharply in the case of 1-naphthol. The system transitions from nearly decoupled to strongly coupled in the small span from $\lambda = 0.333$ to the next larger value at $\lambda = 0.4$. Presumably, at some λ value between these two the two modes are equally probable. However, it would be very difficult to establish accurately the transition point because interconversions from one state to the other are extremely rare (see Figure 5). The reason for this is that the probability of visiting an intermediate state between the weakly coupled and the strongly coupled states is immeasurably small (Figure 2B). In particular, the analytical model trained on this data (see below) predicts a small population of strongly coupled states at $\lambda = 0.333$ and, conversely, a small population of weakly coupled states at $\lambda = 0.4$ (see the minor modes on the gold and green curves in Figure 2B). However, as confirmed by the simulation (Figure 5), even if the prediction is accurate the lack of interconversions between the two states after a transient initial period makes it impossible to accurately estimate their relative equilibrium populations at any λ . Because the free energy is affected by the relative populations of the coupled and uncoupled states as a function of λ ,¹⁵ it is expected (and confirmed, see below) that the hydration free energy estimate for 1-naphthol would be substantially biased in this case.

The data shown in Figure 2 confirms the observed probability distributions of the soft-core solute-solvent interaction energies are accurately reproduced by the analytical model for $p_0(u_{sc})$ ^{11,15} parameterized to each dataset. The maximum

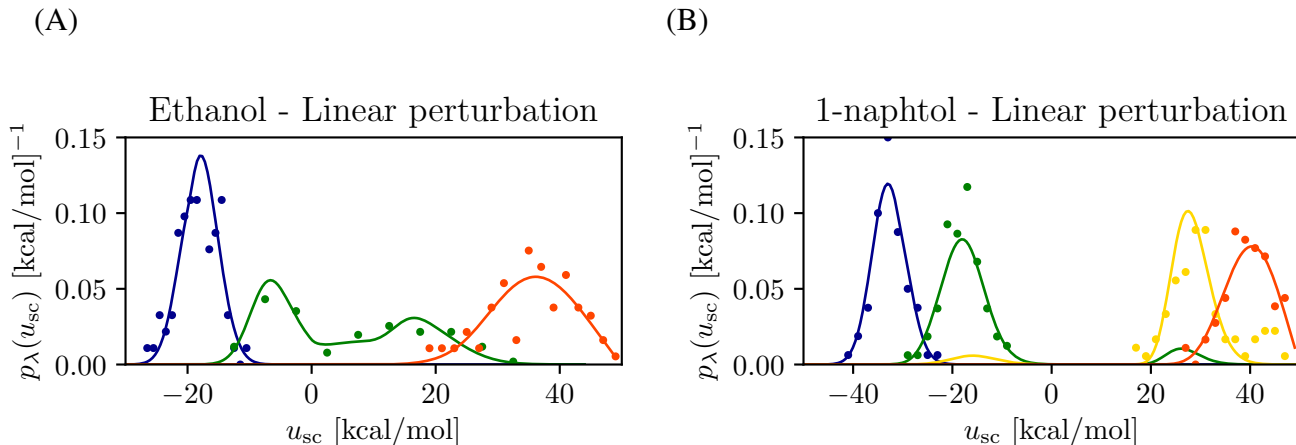


FIG. 2. The predicted (continuous lines) and observed (dots) probability densities of the soft-core solute-solvent interaction energy, $p_\lambda(u_{sc})$, for the alchemical hydration of with the linear perturbation function $W_\lambda(u_{sc}) = \lambda u_{sc}$ for (A) ethanol with (from right to left) $\lambda = 0$ (orange/red), $\lambda = 0.267$ (green), and $\lambda = 1$ (blue), and (B) 1-naphtol with (from right to left) $\lambda = 0$ (orange/red), $\lambda = 0.333$ (gold), $\lambda = 0.4$ (green), and $\lambda = 1$ (blue). The predicted distributions are obtained using the analytical model for $p_0(u_{sc})$, Eqs. (11) to (13)], with the parameters listed in Table II.

likelihood-optimized parameters of the model are listed in Table II. The model reproduces accurately the positions of the distributions and their variations as a function of λ , including the points where transitions occur.

The parameterized analytical functions for $p_0(u_{sc})$ are analytically differentiated with respect to u_{sc} to obtain the corresponding λ -functions $\lambda_0(u_{sc})$ [Eq. (14)]¹¹ shown in Figure 3 for the hydration of ethanol and 1-naphtol. These functions are useful because they can be used to locate, graphically, the maxima and minima of the probability distributions of the soft-core solute-solvent interaction energy as λ is varied. The procedure consists of finding the intersections between the λ -function and, in the case of a linear perturbation potential, the horizontal line drawn at the level of the desired value of λ .

Indeed, the predictions from the λ -functions in Figure 3 are quantitatively consistent with the observations in Figure 2. In each case, near $\lambda = 0$ the distributions are expected to have a single mode at large values of u_{sc} . As λ is increased (that is as the horizontal line is shifted up), a back-bending region³⁰ of the λ -function is encountered in which typically three intersections occur with the first and the last corresponding to maxima of the distributions and the middle one to a minimum. More complex patterns can arise when there are multiple back-bending regions. In the case of ethanol, above a critical value of λ (approximately 0.4) the distributions return to be unimodal at low values of the solute-solvent interaction energies. In the case of 1-naphtol the back-bending of the λ -function is predicted to be so extreme to prevent unimodal distributions for large values of λ less than 1.

While the λ -functions identify the locations of maxima and minima of the distributions, they alone do not predict the relative populations of competing modes. Thus, for example, at $\lambda = 1$ 1-naphtol is overwhelmingly more likely to form favorable interactions with the solvent even though a second,

immeasurably small, mode is predicted to exist at unfavorable interaction energies.

The integrated logistic perturbation potential can be tuned to reduce the perturbation energy gap across the hydration/dehydration transition and to avoid hard-to-converge bimodal distributions.¹¹ As shown in Figure 3(A) the parameters of the integrated logistic potential can be tuned to avoid multiple intersections with the λ -function thereby avoiding the occurrence of bimodal distributions (see below). When this is not possible, as in Figure 3(B), the logistic potential is still useful to reduce the energy gap between competing modes and to favor one mode over another.

The alchemical simulations with the integrated logistic potential with optimized parameters (Table II) designed based on the predicted λ -functions (Figure 3) indeed show the absence of a gap of the solute-solvent interaction energy and a gradual shift of the probability distributions as the solute is coupled to the solvent (see Figure 4, to be compared with Figure 2 with the linear alchemical potential). The distributions with the integrated logistic alchemical potential are also generally unimodal reflecting either lack of multiple modes or the gradual shift from one mode to another as λ is varied. The effect of the integrated logistic potential is smaller in the case of ethanol which does not exhibit a strong hydration transition with the linear potentials. It has, however, a very substantial effect on 1-naphtol where an interaction energy gap of more than 30 kcal/mol (Figure 2B) is virtually eliminated (Figure 4B) thereby facilitating interconversions between the weakly coupled and strongly coupled states (see below).

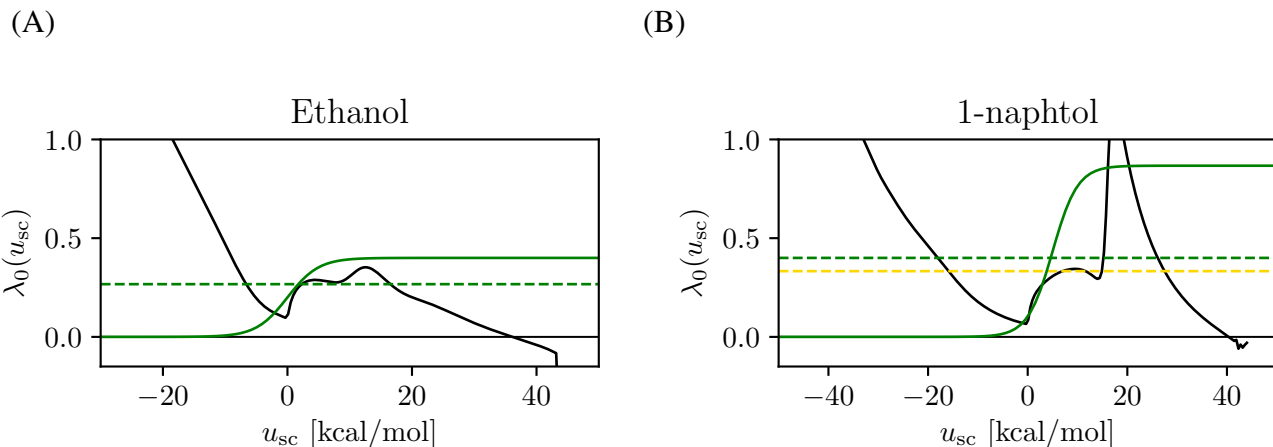


FIG. 3. The predicted λ -functions for the hydration of (A) ethanol and (B) 1-naphtol obtained from the analytical model for $p_0(u_{sc})$ [Eqs. (11) to (13)], and Eq. (14) with the parameters listed in Table II. The dashed horizontal lines correspond to the values of λ where the probability distributions of the soft-core solute solvent energy are predicted to be bimodal [$\lambda = 0.267$ in (A) and $\lambda = 0.333$ and $\lambda = 0.4$ in (B)]. The point of intersections of the horizontal lines correspond to the maxima and minima of the respective distributions (Figure 2).¹¹ The solid sigmoid curve is the derivative, $\partial W_\lambda(u_{sc})/\partial u_{sc}$, of the integrated logistic function for a representative value of λ [$\lambda = 0.6$ for (A) and $\lambda = 0.4$ for (B)].

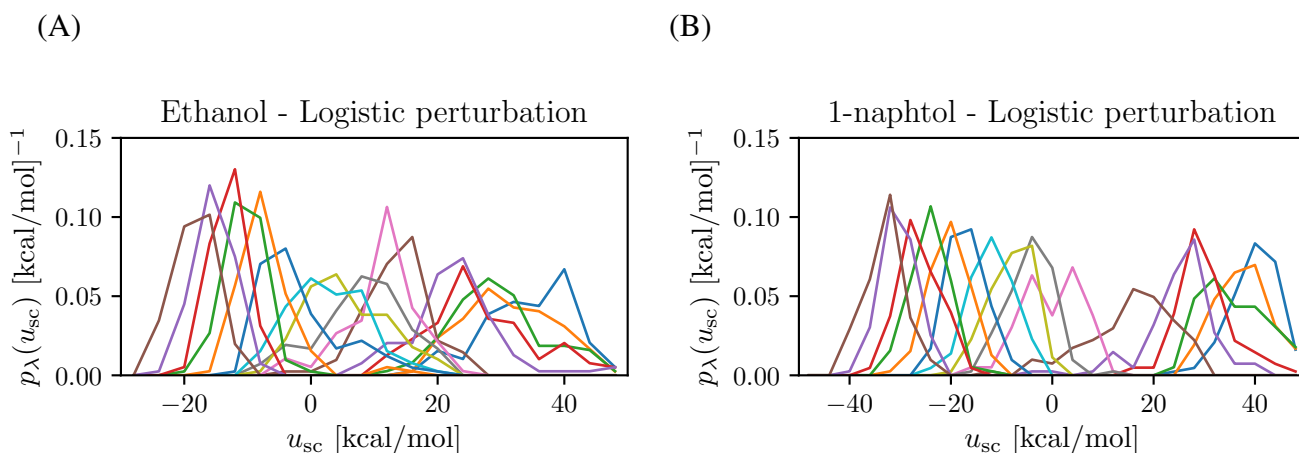


FIG. 4. The probability densities of the soft-core solute-solvent interaction energy from the alchemical simulations with the integrated logistic perturbation potential [Eq. (4)] with the parameters in Table II for the hydration of (A) ethanol and (B) 1-naphtol. The distributions shift from right to left with alternating colors as the λ progress variable progressively varies from 0 (vacuum state) to 1 (hydrated state).

B. Analysis of Replica Exchange Efficiency

Hamiltonian replica exchange efficiency has been monitored here in terms of the extent of diffusion of replicas in solute-solvent interaction energy space. We are particularly interested in the rate of transitions between coupled states with favorable solute-solvent interaction energies and uncoupled states with large and repulsive interaction energy. The time trajectories of the soft-core solute-solvent interaction energies sampled by the replicas are shown in Figure 5. The number of transitions from uncoupled to coupled states (hydration) and vice versa (dehydration) is presented in Table I.

The data indicates that ethanol undergoes frequent hydration/dehydration events with either the linear and integrated logistic perturbation potentials. 1-naphtol however undergoes very few hydration/dehydration transitions and none at all in the latest three quarters of the simulation with the linear perturbation potential. This is due to the wide and strong interaction energy gap between the distributions of solute-solvent interaction energies of states near the coupled state and those near the decoupled state (Figure 2). The bulky nature of this solute makes it very improbable for a decoupled 1-naphtol molecule to find a suitable cavity in the solvent to make favorable interactions with the solvent. Conversely, 1-naphtol in

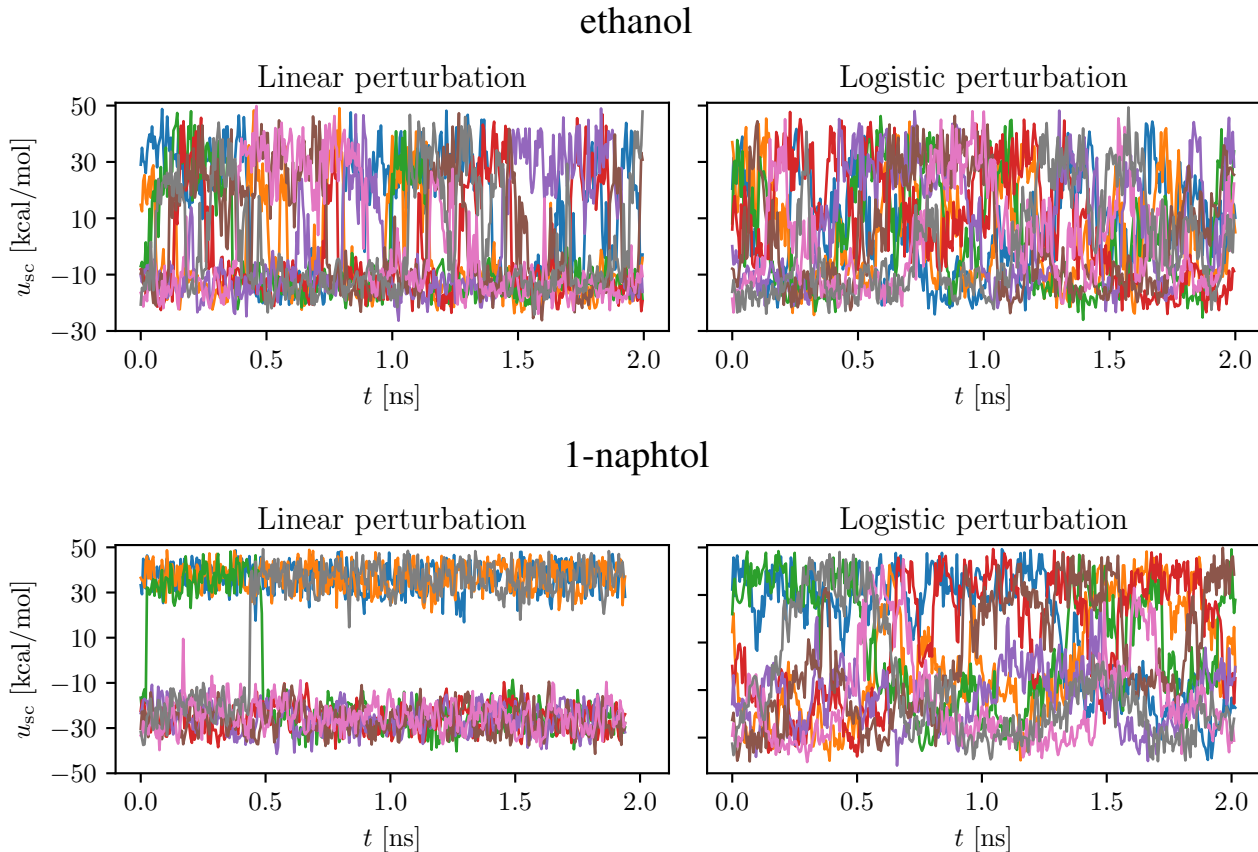


FIG. 5. Soft-core solute-solvent interaction energy trajectories for selected replicas of the alchemical replica exchange simulations of the hydration of ethanol (top) and 1-naphtol (bottom) as a function of simulation time with the linear (left) and integrated logistic (right) alchemical perturbation potentials. Ethanol undergoes multiple hydration and dehydration events with either alchemical perturbation. The bulkier 1-naphtol undergoes frequent hydration and dehydration events only with the integrated logistic perturbation potential.

TABLE I. Number of hydration and dehydration transitions

Protocol	n_{hydr} ethanol ^a	n_{dehydr}
Linear	58	60
Logistic	48	49
	1-naphtol ^b	
Linear	1	3
Logistic	21	23

^a $u_{\text{lower}} = -10$, $u_{\text{upper}} = 25$ kcal/mol

^b $u_{\text{lower}} = -20$, $u_{\text{upper}} = 25$ kcal/mol

a coupled state is unlikely to overcome the energetic penalty necessary to become decoupled from the solvent. The coupled and decoupled states of 1-naphtol are separated by essentially a pseudo first-order phase transition which is entropically frustrated in the hydration direction and energetically frustrated in the dehydration direction.

The integrated logistic perturbation potential on the other hand is very effective at circumventing the phase transition. As shown in Figure 5 and Table I, with the integrated logistic potential 1-naphtol undergoes many hydration and dehydra-

tion transitions. This makes it possible to rapidly equilibrate and converge the hydration free energy estimate for this solute (see below).

C. Equilibration of Hydration Free Energy Estimates

The computed hydration free energy estimates of ethanol and 1-naphtol are plotted in Figure 6 as a function of the amount of data discarded from the start of the simulation (equilibration time). These plots, referred to as reverse cumulative equilibration profiles,^{31–33} are used to determine the equilibration time after which the time series of data generated by the simulation becomes stationary and not biased by the starting conditions. It is not obvious to pin-point such a time because, while the accuracy of the binding free energy presumably improves as more non-equilibrated samples are discarded, the precision of the estimate (illustrated by the error bars in Figure 6) worsens as more initial samples are discarded. Here we take the approach of choosing the hydration free energy estimate with the best compromise between bias and precision as the one corresponding to the smallest equilibration time that gives a value statistically indistinguishable

from those at all subsequent equilibration times.

Based on this criterion, we conclude that the hydration free energy of ethanol equilibrates almost immediately after the start of the simulation with either the linear or integrated logistic alchemical potentials. The two estimates are -2.30 ± 0.14 kcal/mol and -2.16 ± 0.16 kcal/mol for the linear and integrated logistic potentials, respectively, are in statistical agreement. Given the very different nature of the alchemical paths in the two simulations, it must be concluded that equilibration and convergence of the hydration free energy has been achieved in this case. This positive outcome is consistent with the high rate of hydration and dehydration events observed for ethanol (Figure 5 and Table I). It also confirms the validity of the alchemical protocol and the correctness of the simulation algorithms in producing a canonical ensemble of conformations.

The reverse cumulative equilibration profiles paint a different picture for the bulkier 1-naphthol (Figure 6). With the linear perturbation potential the hydration free energy of 1-naphthol appears to equilibrate after approximately 0.75 ns at a value of -3.23 ± 0.25 kcal/mol. With the integrated logistic potential instead, the hydration free energy appears to equilibrate immediately after the start of the simulation at a value of -3.86 ± 0.22 kcal/mol. The two values are most certainly statistical inconsistent (the p -value of being equivalent is 8×10^{-5} based on a simple t -test) and, based on the very few occurrences of hydration/dehydration events (Table I) and the slow equilibration (Figure 6), it can be concluded that the estimate with the linear alchemical potential is the least reliable.

IV. DISCUSSION

Alchemical hydration free energy calculations are widely employed to predict the water solubilities of substances,^{4,34} test force field and free energy protocols,^{35–37} and to estimate absolute and relative binding free energies of molecular complexes.^{3,38} While early alternatives have been proposed,³⁹ the generally accepted guidelines to avoid slow convergence and numerical instabilities are to split the alchemical hydration process in two steps. In the first step volume-exclusion and dispersion solute-solvent interactions are turned on, followed by a second step in which electrostatic interactions are established.⁹ In addition, especially during the first phase, it has been found necessary to employ customized soft-core interatomic pair potentials.^{40,41}

These free energy practices are widely implemented in popular molecular simulation packages,^{22,42–45} and, while generally successful and robust, their equilibration and convergence rates are likely not optimal. In addition their deployment and software implementations can be cumbersome and difficult to integrate and maintain alongside other molecular simulation algorithms. A recent study by Lee et al.¹⁰ discussed the downsides of multi-step free energy methods and called for a streamlined single-step approach that would more easily be integrated with extended ensemble and self-adjusting conformational sampling algorithms and non-equilibrium approaches.^{46,47} Lee et al.¹⁰ furthermore pro-

posed a family of soft-core pair potentials and non-linear alchemical hybrid potentials that enable the calculation of hydration free energies in a single step in which Lennard-Jones and Coulomb interactions are varied in concert rather than separately.

In a recent study¹¹ we identified pseudo first-order phase transitions along the alchemical path as the critical and fundamental obstacles to the application of single-step alchemical processes in which two chemical species are coupled to each other. In the same study, we applied Hamiltonian-shaping techniques inspired by non-Boltzmann sampling methodologies developed by Straub and collaborators^{30,48} for the study of temperature-driven first order phase transitions, to choose an alchemical path that avoids or softens biphasic behavior. In this study we show that the same techniques that we developed earlier in the context of an implicit description of the solvent can be also applied to the estimation of hydration free energies with explicit solvation. This approach not only introduces a new family of alchemical perturbation functions of potentially wide applicability, but it also proposes a theoretical framework and a numerical and graphical procedure to optimize them to systematically improve conformational sampling and the rate of equilibration and convergence of free energy estimates.

The theoretical, algorithmic, and numerical simulation strategies presented and the promising results illustrated here suggest a possible roadmap to streamline and improve alchemical free energy protocols as currently implemented in popular molecular simulation packages. The first suggestion is to replace soft-core pair potentials with, as done here, a soft-core function applied to the raw overall solute-solvent interaction energy (without soft-core modifications) [e.g. using Eqs. (6) and (7)] rather than to each individual atomic pair as currently done. This would effectively replace a $O(N^2)$ operation with a $O(1)$ operation that can be easily executed by a single subroutine external to the complex procedures used to perform pairwise calculations. The processing of the gradients of the alchemical potential would require a $O(N)$ operation but it would still be external and separate from the main pairwise loop.

The second suggestion emerging from this study is the use of a non-linear alchemical perturbation that, like the integrated logistic potential we propose [Eq. 4], judiciously warps the alchemical path in critical regions to avoid phase transitions, while retaining a linear character away from the problematic regions. Furthermore, we suggest the use of the λ -function formalism [Eqs. (14) and (15)] and adaptive maximum likelihood-based approaches to systematically optimize the alchemical schedule and the alchemical perturbation function to enhance equilibration and convergence.

V. CONCLUSIONS

We employ a statistical mechanics theory and an analytic theory of molecular association¹⁵ used previously to optimize a single-decoupling alchemical approach to binding free energy estimation^{11,30} to the computation of hydration free en-

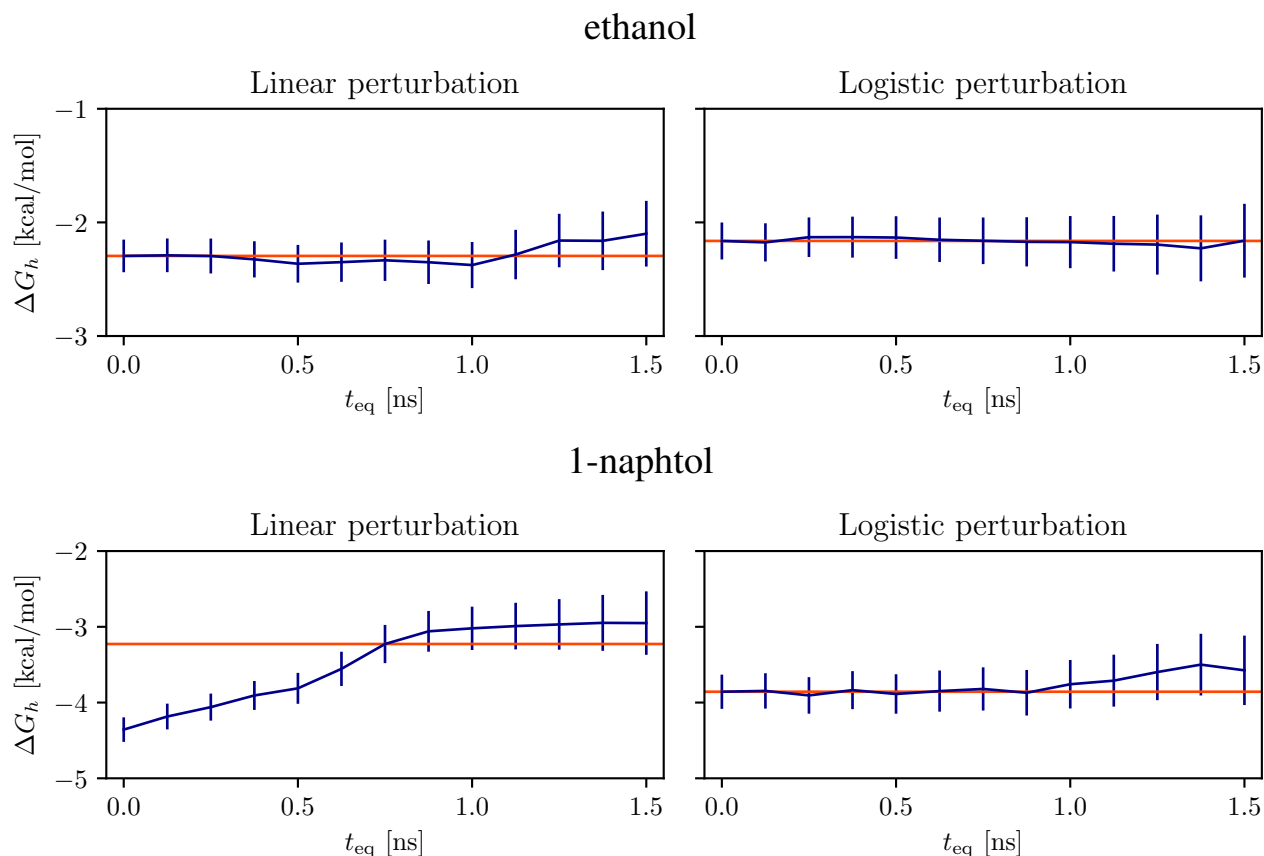


FIG. 6. Reverse cumulative equilibration profiles of the hydration free energies of ethanol (top) and 1-naphthol (bottom) as a function of equilibration time with the linear (left) and integrated logistic (right) alchemical perturbation potentials. The horizontal line corresponds to the last value.

ergies of small to medium-sized molecules. The approach and its benefits are illustrated for a model system involving the hydration of two solutes in a water droplet. This proof of principle study paves the way for a new generation of streamlined and improved single-step free energy estimation algorithms of wide applicability.

ACKNOWLEDGMENTS

We acknowledge support from the National Science Foundation (NSF CAREER 1750511 to E.G.). Molecular simulations were conducted on the Comet GPU supercomputer cluster at the San Diego Supercomputing Center supported by NSF XSEDE award TG-MCB150001.

Appendix A: Appendix

1. Parameters of the Analytical Model for $p_0(u_{sc})$

See Table II.

2. Alchemical Schedule and Parameters of the Integrated Logistic Perturbation Function

See Tables III and IV.

¹A. Ben Naim. *Water and Aqueous Solutions*. Plenum, New York, 1974.

²Christel AS Bergström and Per Larsson. Computational prediction of drug solubility in water-based systems: qualitative and quantitative approaches used in the current drug discovery and development setting. *Inter. J. Pharm.*, 540(1-2):185–193, 2018.

³M. K. Gilson, J. A. Given, B. L. Bush, and J. A. McCammon. The statistical-thermodynamic basis for computation of binding affinities: A critical review. *Biophys. J.*, 72:1047–1069, 1997.

⁴David L Mobley and J Peter Guthrie. Freesolv: a database of experimental and calculated hydration free energies, with input files. *J. Comp. Aid. Mol. Des.*, 28(7):711–720, 2014.

⁵Chipot and Pohorille (Eds.). *Free Energy Calculations. Theory and Applications in Chemistry and Biology*. Springer Series in Chemical Physics. Springer, Berlin Heidelberg, Berlin Heidelberg, 2007.

⁶Anita de Ruiter and Chris Oostenbrink. Free energy calculations of protein–ligand interactions. *Current opinion in chemical biology*, 15(4):547–552, 2011.

⁷Thomas Simonson. Free energy of particle insertion: an exact analysis of the origin singularity for simple liquids. *Molecular Physics*, 80(2):441–447, 1993.

⁸David L Mobley. Lets get honest about sampling. *J. Comp. Aided Mol. Des.*, 26:93–95, 2012.

- ⁹Pavel V Klimovich, Michael R Shirts, and David L Mobley. Guidelines for the analysis of free energy calculations. *J. Comp. Aid. Mol. Des.*, 29(5):397–411, 2015.
- ¹⁰Tai-Sung Lee, Zhixiong Lin, Bryce K Allen, Charles Lin, Brian K Radak, Yujun Tao, Hsu-Chun Tsai, Woody Sherman, and Darrin M York. Improved alchemical free energy calculations with optimized smoothstep softcore potentials. *J. Chem. Theory Comput.*, 2020.
- ¹¹Rajat K Pal and Emilio Gallicchio. Perturbation potentials to overcome order/disorder transitions in alchemical binding free energy calculations. *J. Chem. Phys.*, 151(12):124116, 2019.
- ¹²Michael R Shirts and John D Chodera. Statistically optimal analysis of samples from multiple equilibrium states. *J. Chem. Phys.*, 129:124105, 2008.
- ¹³Zhiqiang Tan, Emilio Gallicchio, Mauro Lapelosa, and Ronald M. Levy. Theory of binless multi-state free energy estimation with applications to protein-ligand binding. *J. Chem. Phys.*, 136:144102, 2012.
- ¹⁴E. Gallicchio, M. M. Kubo, and R. M. Levy. Entropy-enthalpy compensation in solvation and ligand binding revisited. *J. Am. Chem. Soc.*, 120:4526–27, 1998.
- ¹⁵Denise Kilburg and Emilio Gallicchio. Analytical model of the free energy of alchemical molecular binding. *J. Chem. Theory Comput.*, 14(12):6183–6196, 2018.
- ¹⁶Emilio Gallicchio, Mauro Lapelosa, and Ronald M. Levy. Binding energy distribution analysis method (BEDAM) for estimation of protein-ligand binding affinities. *J. Chem. Theory Comput.*, 6:2961–2977, 2010.
- ¹⁷Emilio Gallicchio and Ronald M Levy. Recent theoretical and computational advances for modeling protein-ligand binding affinities. *Adv. Prot. Chem. Struct. Biol.*, 85:27–80, 2011.
- ¹⁸Martín Abadi, Ashish Agarwal, Paul Barham, Eugene Brevdo, Zhifeng Chen, Craig Citro, Greg S. Corrado, Andy Davis, Jeffrey Dean, Matthieu Devin, Sanjay Ghemawat, Ian Goodfellow, Andrew Harp, Geoffrey Irving, Michael Isard, Yangqing Jia, Rafal Jozefowicz, Lukasz Kaiser, Manjunath Kudlur, Josh Levenberg, Dandelion Mané, Rajat Monga, Sherry Moore, Derek Murray, Chris Olah, Mike Schuster, Jonathon Shlens, Benoit Steiner, Ilya Sutskever, Kunal Talwar, Paul Tucker, Vincent Vanhoucke, Vijay Vasudevan, Fernanda Viégas, Oriol Vinyals, Pete Warden, Martin Wattenberg, Martin Wicke, Yuan Yu, and Xiaoqiang Zheng. TensorFlow: Large-scale machine learning on heterogeneous systems, 2015. Software available from tensorflow.org.
- ¹⁹Tai-Sung Lee, Brian K Radak, Anna Pabis, and Darrin M York. A new maximum likelihood approach for free energy profile construction from molecular simulations. *J. Chem. Theory Comput.*, 9(1):153–164, 2012.
- ²⁰Albert C Pan, Huafeng Xu, Timothy Palpant, and David E Shaw. Quantitative characterization of the binding and unbinding of millimolar drug fragments with molecular dynamics simulations. *J. Chem. Theory Comput.*, 13(7):3372–3377, 2017.
- ²¹Junmei Wang, Romain M Wolf, James W Caldwell, Peter A Kollman, and David A Case. Development and testing of a general amber force field. *J. Comp. Chem.*, 25(9):1157–1174, 2004.
- ²²Peter Eastman, Jason Swails, John D Chodera, Robert T McGibbon, Yutong Zhao, Kyle A Beauchamp, Lee-Ping Wang, Andrew C Simmonett, Matthew P Harrigan, Chaya D Stern, et al. Openmm 7: Rapid development of high performance algorithms for molecular dynamics. *PLoS Comp. Bio.*, 13(7):e1005659, 2017.
- ²³Emilio Gallicchio, Junchao Xia, William F Flynn, Baofeng Zhang, Sade Samlalsingh, Ahmet Mentesh, and Ronald M Levy. Asynchronous replica exchange software for grid and heterogeneous computing. *Computer Physics Communications*, 196:236–246, 2015.
- ²⁴Yuji Sugita, Akio Kitao, and Yuko Okamoto. Multidimensional replica-exchange method for free-energy calculations. *J. Chem. Phys.*, 113:6042–6051, 2000.
- ²⁵A. K. Felts, Y. Harano, E. Gallicchio, and R. M. Levy. Free energy surfaces of beta-hairpin and alpha-helical peptides generated by replica exchange molecular dynamics with the AGBNP implicit solvent model. *Proteins: Struct. Funct. Bioinf.*, 56:310–321, 2004.
- ²⁶K.P. Ravindranathan, E. Gallicchio, R. A. Friesner, A. E. McDermott, and R. M. Levy. Conformational equilibrium of cytochrome P450 BM-3 complexed with N-palmitoylglycine: A replica exchange molecular dynamics study. *J. Am. Chem. Soc.*, 128:5786–5791, 2006.
- ²⁷Hisashi Okumura, Emilio Gallicchio, and Ronald M Levy. Conformational populations of ligand-sized molecules by replica exchange molecular dynamics and temperature reweighting. *J. Comput. Chem.*, 31:1357–1367, 2010.
- ²⁸Christopher J. Woods, Jonathan W. Essex, and Michael A. King. The development of replica-exchange-based free-energy methods. *J. Phys. Chem. B*, 107:13703–13710, 2003.
- ²⁹Steven W. Rick. Increasing the efficiency of free energy calculations using parallel tempering and histogram reweighting. *J. Chem. Theory Comput.*, 2:939–946, 2006.
- ³⁰Jaegil Kim and John E Straub. Generalized simulated tempering for exploring strong phase transitions. *J. Chem. Phys.*, 133(15):154101, 2010.
- ³¹Wei Yang, Ryan Bitetti-Putzer, and Martin Karplus. Free energy simulations: use of the reverse cumulative averaging to determine the equilibrated region and the time required for convergence. *J. Chem. Phys.*, 120(6):2618–2628, 2003.
- ³²John D Chodera. A simple method for automated equilibration detection in molecular simulations. *J. Chem. Theory Comput.*, 12(4):1799–1805, 2016.
- ³³Denise Kilburg and Emilio Gallicchio. Assessment of a single decoupling alchemical approach for the calculation of the absolute binding free energies of protein-peptide complexes. *Frontiers in Molecular Biosciences*, 5:22, 2018.
- ³⁴Tang-Qing Yu, Pei-Yang Chen, Ming Chen, Amit Samanta, Eric Vanden-Eijnden, and Mark Tuckerman. Order-parameter-aided temperature-accelerated sampling for the exploration of crystal polymorphism and solid-liquid phase transitions. *J. Chem. Phys.*, 140(21):06B603_1, 2014.
- ³⁵David L Mobley, Shuai Liu, David S Cerutti, William C Swope, and Julia E Rice. Alchemical prediction of hydration free energies for sampl. *J. Comp. Aid. Mol. Des.*, 26(5):551–562, 2012.
- ³⁶David L Mobley, Elise Dumont, John D Chodera, and Ken A Dill. Comparison of charge models for fixed-charge force fields: small-molecule hydration free energies in explicit solvent. *J Phys Chem B*, 111:2242–2254, 2007.
- ³⁷Devleena Shivakumar, Joshua Williams, Yujie Wu, Wolfgang Damm, John Shelley, and Woody Sherman. Prediction of absolute solvation free energies using molecular dynamics free energy perturbation and the oplf force field. *J. Chem. Theory Comput.*, 6(5):1509–1519, 2010.
- ³⁸John D. Chodera, David L. Mobley, Michael R. Shirts, Richard W. Dixon, Kim Branson, and Vijay S. Pande. Alchemical free energy methods for drug discovery: Progress and challenges. *Curr. Opin. Struct. Biol.*, 21:150–160, 2011.
- ³⁹Clara D Christ and Wilfred F van Gunsteren. Multiple free energies from a single simulation: Extending enveloping distribution sampling to nonoverlapping phase-space distributions. *The Journal of chemical physics*, 128(17):174112, 2008.
- ⁴⁰Jed W Pitera and Wilfred F van Gunsteren. A comparison of non-bonded scaling approaches for free energy calculations. *Molecular Simulation*, 28(1-2):45–65, 2002.
- ⁴¹Thomas Steinbrecher, InSuk Joung, and David A. Case. Soft-core potentials in thermodynamic integration: Comparing one- and two-step transformations. *J. Comput. Chem.*, 32:3253–3263, 2011.
- ⁴²Bernard R Brooks, Charles L Brooks III, Alexander D Mackerell Jr, Lennart Nilsson, Robert J Petrella, Benoît Roux, Youngdo Won, Georgios Archontis, Christian Bartels, Stefan Boresch, et al. Charmm: the biomolecular simulation program. *Journal of computational chemistry*, 30(10):1545–1614, 2009.
- ⁴³James C Phillips, Rosemary Braun, Wei Wang, James Gumbart, Emad Tajkhorshid, Elizabeth Villa, Christophe Chipot, Robert D Skeel, Laxmikant Kale, and Klaus Schulten. Scalable molecular dynamics with namd. *J. Comp. Chem.*, 26(16):1781–1802, 2005.
- ⁴⁴Sander Pronk, Szilárd Páll, Roland Schulz, Per Larsson, Pär Bjelkmar, Rossen Apostolov, Michael R Shirts, Jeremy C Smith, Peter M Kasson, David van der Spoel, Berk Hess, and Erik Lindahl. Gromacs 4.5: a high-throughput and highly parallel open source molecular simulation toolkit. *Bioinformatics*, 29:845–854, 2013.
- ⁴⁵Xibing He, Shuhan Liu, Tai-Sung Lee, Beihong Ji, Viet H Man, Darrin M York, and Junmei Wang. Fast, accurate, and reliable protocols for routine calculations of protein–ligand binding affinities in drug design projects using AMBER GPU-TI with ff14SB/GAFF. *ACS Omega*, 5(9):4611–4619, 2020.

⁴⁶Eric Darve, David Rodríguez-Gómez, and Andrew Pohorille. Adaptive biasing force method for scalar and vector free energy calculations. *The Journal of chemical physics*, 128(14):144120, 2008.

⁴⁷Piero Procacci. Solvation free energies via alchemical simulations: let's get honest about sampling, once more. *Phys. Chem. Chem. Phys.*, 2019.

⁴⁸Qing Lu, Jaegil Kim, and John E Straub. Order parameter free enhanced sampling of the vapor-liquid transition using the generalized replica exchange method. *J. Chem. Phys.*, 138(10):104119, 2013.

TABLE II. Optimized parameters for the analytical model of molecular association for the two systems studied in this work. Uncertainties are implied by the number of reported significant figures.

	weight	p_b	\bar{u}_b^a	σ_b^a	ϵ^a	\tilde{u}^a	n_l
			ethanol hydration				
mode 1	3.55×10^{-3}	1.88×10^{-6}	-7.30	2.65	3.75	-1.69	4.78
mode 2	2.07×10^{-1}	8.89×10^{-7}	-4.51	2.65	22.6	30.3	4.70
mode 3	7.90×10^{-1}	1.88×10^{-9}	9	1.7	15.6	85	9.1
			1-naphtol hydration				
mode 1	1.94×10^{-8}	9.31×10^{-8}	-15.35	3.24	4.93	2.52	4.87
mode 2	2.31×10^{-7}	6.13×10^{-8}	-10.70	3.22	7.91	15.1	6.10
mode 3	1.00	1×10^{-20}	13.7	3	18.5	72	17.5

^a In kcal/mol

TABLE III. Alchemical schedule of the integrated logistic perturbation function for the hydration of ethanol

λ	λ_1	λ_2	α^a	u_0^b	w_0^c
0.000	0.000	0.000	0.400	10.000	0.000
0.067	0.000	0.044	0.400	10.000	-0.521
0.133	0.000	0.089	0.400	10.000	-1.043
0.200	0.000	0.133	0.400	10.000	-1.564
0.267	0.000	0.178	0.400	10.000	-2.086
0.333	0.000	0.400	0.400	8.889	-4.249
0.400	0.000	0.400	0.400	6.667	-3.360
0.467	0.000	0.400	0.400	4.444	-2.471
0.533	0.000	0.400	0.400	2.222	-1.582
0.600	0.000	0.400	0.400	0.000	-0.693
0.667	0.167	0.400	0.400	0.000	-0.404
0.733	0.333	0.400	0.400	0.000	-0.116
0.800	0.500	0.500	0.400	0.000	0.000
0.867	0.667	0.667	0.400	0.000	0.000
0.933	0.833	0.833	0.400	0.000	0.000
1.000	1.000	1.000	0.400	0.000	0.000

^a kcal/mol⁻¹^b kcal/mol^c kcal/mol

TABLE IV. Alchemical schedule of the integrated logistic perturbation function for the hydration of 1-naphtol

λ	λ_1	λ_2	α^a	u_0^b	w_0^c
0.000	0.000	0.000	0.400	5.000	0.000
0.067	0.000	0.116	0.400	5.000	-0.778
0.133	0.000	0.231	0.400	5.000	-1.557
0.200	0.000	0.347	0.400	5.000	-2.335
0.267	0.000	0.462	0.400	5.000	-3.113
0.333	0.000	0.578	0.400	5.000	-3.892
0.400	0.000	0.867	0.400	5.000	-5.837
0.467	0.000	0.867	0.400	1.667	-2.947
0.533	0.067	0.867	0.400	0.000	-1.387
0.600	0.200	0.867	0.400	0.000	-1.156
0.667	0.333	0.867	0.400	0.000	-0.925
0.733	0.467	0.867	0.400	0.000	-0.694
0.800	0.600	0.867	0.400	0.000	-0.463
0.867	0.733	0.867	0.400	0.000	-0.232
0.933	0.867	0.867	0.400	0.000	0.000
1.000	1.000	1.000	0.400	0.000	0.000

^a kcal/mol⁻¹^b kcal/mol^c kcal/mol